EFFECTS OF FREE-CUTTING ELEMENTS ADDITION ON THE MICROSTRUCTURE, HARDNESS, AND MACHINABILITY OF Al-11%Si–Cu–Mg CASTING ALLOYS

Y. Zedan and V. Songmene
École de technologie supérieure, Montréal, QC, Canada

A. M. Samuel and F. H. Samuel
Université du Québec à Chicoutimi, Saguenay, QC G7H 2B1, Canada

H. W. Doty
General Motors Materials Engineering, Pontiac, MI, USA

https://doi.org/10.1007/s40962-021-00740-2

Abstract

The addition of small but effective amounts of free-machining elements to Al–Si casting alloys significantly improves the machinability of these alloys. These added elements, which are softer and have a lower melting point than the matrix alloy, form as small globules dispersed in the microstructure of the aluminum casting. In this form, the dispersed phase of low-melting elements promotes chip-breaking and helps to lubricate the cutting tool. The Al-11%Si-Cu-Mg alloys studied were mechanically tested in order to acquire an understanding of the effects of additives on the tensile properties under the same alloy conditions used for preparing the machinability test blocks. Drilling operations were carried out using a high-speed machining center under fixed cutting conditions. The machinability characteristics of these alloys were evaluated by examining the drilling forces and moments, tool life, and chip shape in each case. Results show that the addition of 0.15wt% Sn has a beneficial effect on the tool life of carbide drills, which may be ascribed to the precipitation of small and uniformly distributed β-Sn particles having a low melting point. Lead is not a suitable choice as an additive because of environmental concerns. Bismuth also has several detrimental effects associated with its presence in the Al–Si alloys, including the formation of the high melting point Bi_2Mg_3 phase, and the interaction of Bi with Sr, which is mainly added/required for Si modification. Thus, of the free-machining elements tested, Sn is the most promising in the context of improving the alloy machinability and mechanical properties.

Keywords: *396 aluminum alloys, Pb, Bi, Sn additions, microstructure, cutting forces, tool life, machinability*

Introduction

Aluminum alloys with a high weight percentage of silicon (Si) are widely used in the automotive industry, and Si is the alloying element that sustains the aluminum casting industry. It is customary within the casting manufacturing process to obtain near-net-shape geometries, which are most often submitted to machining operations in order to meet the necessary dimensional tolerance requirements. The change of flake-like eutectic silicon into the refined lamellar structure increased surface roughness and decreased the machinability of Al–12Si–2Cu cast alloy. However, the formation of Bi compound that acts as a lubricant during turning can be more likely a reason to obtain the best surface roughness and lowest main cutting force value compared to the base and Sr-containing workpieces. Traditional processes, i.e., additive manufacturing technologies, offer significant benefits, such as near-net-shape production capabilities, superior design and geometrical flexibility, reduced tooling, shorter cycle time for design and manufacturing, as well as material, energy and cost efficiency. Sustainable machining can be considered to link with the transformation of input materials and

Received: 10 October 2021 / Accepted: 06 December 2021 /
Published online: 5 January 2022

energy/power demand into finished goods. Machining processes are responsible for environmental effects accepting to their power consumption. The cutting conditions have been optimized to minimize the cutting power, which is the power consumed for cutting.[1–19]

One of the important aspects of machining is the measurement of the cutting forces acting on the tool.[20] Adhesion of aluminum to the face of the cutting tool increases the build-up edge (BUE) that in turn changes the tool geometry and increases the roughness of the new surface.[21] The size of BUE is greater when the bifilm index is high.[22] A higher population of oxides and inclusions will result in increased BUE, which can be predicted by bifilm index. Chip shape is the most important factor in obtaining the smoothness of the drilling process, which will proceed easily if the chips are well-broken. Most ductile materials, however, do not break during drilling and form continuous chips instead.[21] Chips, their length and curl, and the ease or difficulty associated with their removal and handling influence the surface finish. The main problems arising in the drilling of aluminum cast alloys are considered to be the adhesion, or welding, of the chip to the drill with the concomitant chip-flute clogging. All of these problems are closely related to the process of chip formation and chip removal within the flute itself. Therefore, chip form is often used to assess the machinability of soft, ductile alloys, especially aluminum alloys.[22]

One of the approaches suitable for improving machinability is the use of free-cutting alloys; these are developed from standard heat-treatable alloys to which elements have been added to form additional phases in the aluminum matrix. These phases improve the machinability of any given material because they provide a smooth surface, cause less tool wear, and produce chips, which are more easily breakable.[23,24] Free-cutting constituents tend to form in the presence of alloying elements and display the following properties: (i) they are insoluble in both liquid and solid aluminum, (ii) they have a low melting point with regard to aluminum, (iii) they do not form intermetallic compounds with aluminum or other alloying elements, and (iv) they have lower hardness values compared to the aluminum matrix. These conditions may be fulfilled by using lead (Pb), bismuth (Bi), tin (Sn), cadmium (Cd), indium (In), antimony (Sb), and a number of other elements which are, however, unusable from a practical point of view[25,26]

It should be mentioned here that most of the work carried out to date on free-machining aluminum alloys has involved wrought alloys. Only a few studies have dealt with cast alloys, producing conflicting results. Jorstad [27] added Pb, Sn, or Bi to A380 alloy as lubricating elements, but observed that no beneficial effect accrued in the form of decreased friction or attenuated tool wear. Alabi et al.[28] and Mohamed et al.[29] successfully added Bi or Bi–Sn to an Al–Si alloy used for air-conditioning components, not for machinability reasons, but to reduce friction in the component. Zaima *et al.*[20] reported that cutting efficiency was observed to improve in Al-13%Si alloys containing $0.2 \sim 0.4\%$ Sn in that there was a decrease in cutting resistance, the cutting temperature was lowered, and the process of tool wear was slowed down. The improvement in machined surfaces was not clearly defined, although the treatment of chips became easier because their shape had undergone a transformation into a sheared form. On the other hand, in Al-23%Si alloys containing the same level of tin, *i.e.,* about 0.2–0.4%Sn, the improvement in machinability was negligible. Neither the decrease in cutting force nor the drop in cutting temperature was at all obvious. The effects of the addition of tin on tool wear and machined surfaces were also not distinct. The chip shape of the original alloy was likely to be a sheared form, and the alloy containing tin produced finer chips of a similar shape.[30,31]

Bismuth, a highly reactive element, reacts not only with Sr, Na, and Ca, which themselves contribute to the modification of the Si-phase, but also with Ni and Mg, which are normally added to increase the strength of the alloy, so that the effectiveness of these elements ultimately decreases, as do the mechanical properties of the alloy.[1] Cho and Loper[23] demonstrated that bismuth in Al–Si alloys interacts with major modifiers, such as sodium and strontium. They postulated that the formation of a ternary Bi-Mg-Sr compound (Bi_2Mg_2Sr) and/or binary Bi–Sr compounds (Bi_3Sr, BiSr, Bi_2Sr_3, and $BiSr_2$) would occur as a result. The Bi-phase, however, does not form an intermetallic compound with Al because it is independently distributed. Thus, the Bi-phase is not uniformly distributed throughout the Al–Si alloy structure, and it also has a tendency to segregate, thereby forming a coarse phase.[32]

Lead (Pb) was used for the purposes of this study because it has already been recognized as a free-machining element. It is considered that the addition of Pb to aluminum alloys is the most appropriate method for improving machinability, while the process of adding Pb to 2xxx and 6xxx series alloys is already fairly well advanced; the recent work has, however, involved replacing Pb in free-machining wrought alloys with more environmentally friendly additives such as Sn or Bi based on new ecologically oriented criteria.[33] In fact, Pb has been found to be either equivalent to, or even more effective than, tin as a soft-phase alloying addition made to aluminum and its alloys. Some unfavorable factors, however, such as the wide miscibility gap, large range of solidification, and high disparity in the densities of aluminum and lead cause practical problems in the preparation of Pb-containing alloys with a uniform distribution of lead.[34,35]

Consequently, in view of the above, the purpose of this study was to examine the near-eutectic Al–Si cast alloys

containing ~11% Si, namely 396 alloys, as a basis for understanding the role of the three free-machining elements Sn, Bi, and Pb, on the hardness, tensile properties, and machinability of these alloys. It should be mentioned here that the pertinent machinability criteria relate to the total cutting forces and moments, tool life expressed as the number of holes drilled up to point of tool breakage, and chip configuration. A thorough understanding of the role of these elements in the alloys studied would make it possible to select material and workpiece design for obtaining optimum machining combinations conducive to maximum productivity.

Experimental Procedures

Alloy Preparation and Casting Procedures

The as-received 396 ingots were cut into smaller pieces, dried, and melted in charges of 100kg each for the preparation of the various alloy compositions. Melting was carried out in a SiC crucible of 120-kg capacity, using an electrical resistance furnace in which the melting temperature was maintained at 750±5 °C. All the alloys were grain-refined by adding 0.12 wt% Ti as Al-5%Ti-1%B in rod form and modified by adding 200 ppm Sr in the form of an Al-10%Sr master alloy by means of a perforated graphite bell. Taking the grain-refined and modified alloy, coded M1, as a reference, additions of Sn, Bi, and Pb[36–38] were then made to the M1 alloy to study the effects of these elements on the mechanical properties and machinability characteristics of the grain-refined and modified alloy. The melt was degassed for ~15–20 min by means of a graphite impeller rotating at ~150 rpm, using pure dry argon at a gas flow rate of 0.4 m^3/hr, to ensure an homogenous mixing of the additives. It should be noted that, for all the castings involved, the humidity level was between 18 and 20%. The surface oxides and inclusions were skimmed off carefully prior to pouring. Samplings for chemical analysis were also taken concurrently for each melt condition; the chemical analysis was carried out using arc spark spectrometric analysis. The averages obtained for three different chemical analysis samples and the respective codes for the various alloys prepared from the base 396 alloy are listed in Table 1.

The degassed melt was poured into a graphite-coated waffle-plate metallic mold (38 x 170 x 300 mm), which had been preheated to 450 °C to prepare the castings for machinability studies; eighteen machinability test blocks were cast. The test blocks were subsequently cut from each casting and then machined to the final testing form having the overall dimensions of 300mm length, 175mm width, and 30mm thickness, with five ribs each approximately 25mm wide, separated by gaps of 16mm. Prior to casting, RPT test was performed to check on the porosity level. In some cases, random castings were radiographically examined.

Tensile test bars were produced by pouring the degassed molten metal at 450 °C into a preheated permanent steel mold, type ASTM B-108; each mold casting provided two tensile bars, each with a gauge length of 50mm and a cross-sectional diameter of 12.7mm. Five bars were prepared for each alloy composition. The test bars were solution heat-treated at 490 °C for 8h, then quenched in warm water at 65 °C, followed by artificial aging at 200 °C for 5 h (*i.e.*, T6-tempered). The heat-treated test bars were pulled to fracture at room temperature at a strain rate of 4 x 10^{-4} /s using a servohydraulic MTS Mechanical Testing machine.

The heat treatments were selected in such a way as to establish the hardness level as a common factor for all the alloys studied, within the range of 110 ± 10 BHN.[39] This range is the one most frequently used in the majority of commercial applications for aluminum alloys. Solution heat treatments were carried out at 490 °C /8h for the 396 alloys. The solution heat-treated samples were quenched in warm water at 65 °C, followed by artificial aging at 200 °C for 5 hours, *i.e.*, the samples were T6-tempered. Both solution and aging heat treatments were carried out in a forced-air electric furnace with a programmable temperature controller accurate to within ± 2 °C.

Metallographic and Hardness Tests

Samples measuring 25mm x 25mm for metallographic examination were sectioned from the machinability test castings and mounted in bakelite using a mounting press The eutectic silicon–particle characteristics, including

Table 1. Average Chemical Composition of the Alloys Used in this Study

Alloy code	Element % wt)											
	Si	Fe	Cu	Mn	Mg	Pb	Sn	Ti	Bi	Sr	Al	Mn/Fe
M1	11.38	0.46	2.22	0.54	0.33	0.0	0.00	0.16	0.00	0.018	84.8	1.17
M2	11.32	0.46	2.26	0.52	0.34	0.0	0.15	0.17	0.00	0.023	84.6	1.13
M7	10.97	0.46	2.28	0.59	0.38	0.0	0.00	0.13	0.50	0.019	84.5	1.28
M8	10.70	0.37	2.33	0.56	0.29	0.79	0.00	0.29	0.00	0.024	84.4	1.48

particle area, length, roundness (%), aspect ratio, and density (particles/mm^2), were measured and quantified using an image analyzer in conjunction with an optical microscope. The various phases observed were identified using an electron probe microanalyzer (EPMA) coupled with energy-dispersive X-ray (EDX) and wavelength-dispersive spectroscopic (WDS) facilities, operating at 20kv and 30nA, with an electron beam size of $\sim$2 μm.

Hardness measurements were taken on the heat-treated samples using a Brinell hardness tester, with a steel ball of 10 mm diameter and a load of 500 kg applied for 30s. Four blocks were randomly selected from among the eighteen test blocks prepared for each alloy condition. The Brinell hardness value for each test block represents the average of at least forty indentation readings obtained from both faces of the five ribs, namely four indentations per rib face for such a block. The average hardness value for the four blocks selected per alloy was then obtained and designated as representing the hardness value for that alloy condition - Figure 1a.

Tensile test bars were produced by pouring the degassed molten metal at 450 °C into a preheated permanent steel mold, type ASTM B-108, which provided two tensile bars per casting, each with a gauge length of 50mm and a cross-sectional diameter of 12.7mm. Five bars were prepared for each alloy composition. The heat-treated test bars were pulled to fracture at room temperature at a strain rate of 4 x 10^{-4} /s using a servohydraulic mechanical testing machine. The average YS, %El, and UTS values obtained from the five samples tested were considered to be the values representing a specified alloy/condition. It should be kept in mind that all of these alloys were mechanically tested in order to acquire an understanding of the effects of the additives on the mechanical properties at the same specific T6 heat-treated conditions, which were applied to the machinability test blocks.

Machining Procedures

All alloy conditions were tested under the same cutting parameters for drilling and tapping tests. The drilling tests were carried out at rotational speeds of 11000rpm using a feed rate of 1.117m/min with each hole being 28.38mm deep. The tapping tests were conducted at low cutting speeds, *i.e.*, 400rpm, using a feed rate of 0.56m/min with each tapped hole being 20.76mm deep. The cutting parameters for drilling and tapping tests are listed in Table 2.

Drilling tests were performed using a Makino A88E high-speed horizontal machining center with a maximum power of 40 HP (30 kW) and a maximum rotation speed of 18,000 rpm under fixed machining conditions of speed, feed, length of cut, tool type, and coolant as applied to the examination of the alloys under discussion. The experimental setup consisted of an A88E machine, a dynamometer with four sensors, charge amplifiers, and an A/D converter; this setup was applied for the online measurement of drilling forces and moments, while a toolmaker's microscope was used for observing tool-wear characteristics. The drilling tests were carried out at rotational speeds of 11,000 rpm using a feed rate of 1.117m/min with each hole being 28.38mm deep. A synthetic metalworking fluid concentrate composed of 5% cutting fluid + 95% liquid, known as CIMTECH® 310, was pumped at high pressure through the drill to ensure adequate cooling and chip evacuation.

The measuring system using piezoelectric force differs from other methods of measurement. The cutting forces acting on the quartz crystal elements are converted to a proportional electric charge in Pico-Coulombs (PC). A Kistler, model 9255B, 6-component piezoelectric quartz crystal dynamometer was used during drilling and tapping tests for the online measurement of the cutting forces and moments. Each of the sensors has three pairs of quartz plates, one sensitive to pressure in the z direction and the other two pairs responsive to shear in the x and y directions, respectively. The four sensors of the dynamometer, therefore, provide eight electric charges corresponding to the values of the eight components of the cutting forces in the x, y, and z directions, namely Fx_{1+2}, Fx_{3+4}, Fy_{1+4}, Fy_{2+3}, Fz_1, Fz_2, Fz_3, and Fz_4.

The output charges from the dynamometer were guided by an amplifier through the eight-core connecting cables, type 1677A5/16779A5. The charge amplifier converts these charges into proportional voltage signals, which are subsequently converted into force signals by an analog-to-digital (A/D) converter using a data acquisition system. These force signals are independently monitored and recorded for each test block in the LabVIEW program where Cut Pro 8.0 software was used for cutting force measurements. Figure 1 shows the experimental setup, which was organized, including a Kistler dynamometer, charge amplifiers, an A/D converter, and a LabVIEW program for the measurement of the drilling and tapping forces. A toolmaker's microscope was used to examine the build-up edge (BUE) evolution and tool wear characteristics; also, a Go/No-Go gauge test was applied to assess the dimensional accuracy control for both drilled and tapped holes.

Results and Discussion

Microconstituents of 396 Base Alloy

The microstructure of the modified grain-refined and T6 heat-treated 396-M1 (Al-11%Si) alloy is shown in Figure 1a. Eutectic silicon particles that precipitated in the

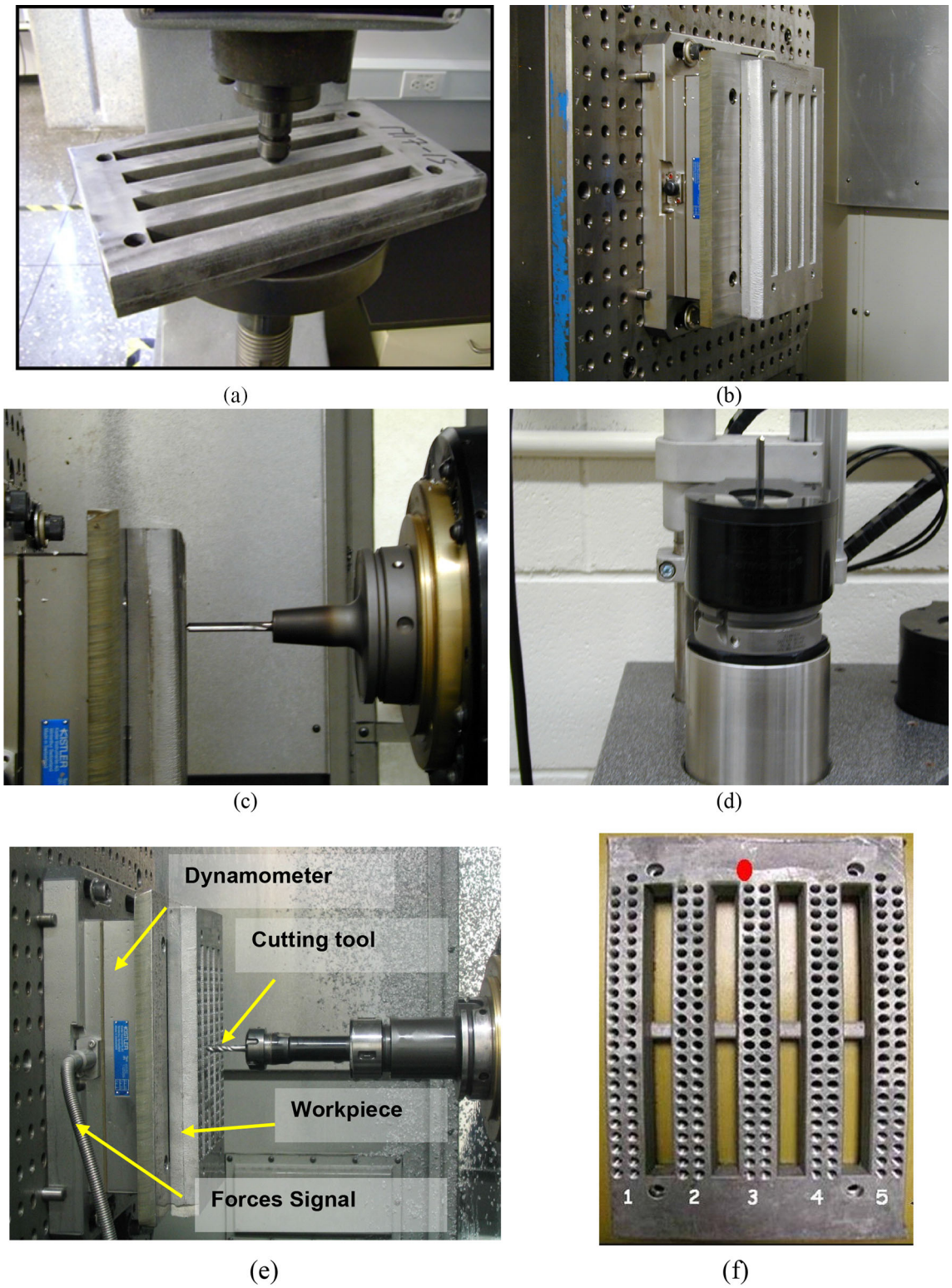

Figure 1. Drilling and tapping experimental setup: (a) hardness measuring, (b) sample and dynamometer cable setup, (c) horizontal machining setup, (d) tool removal during cooling cycle, (e) photograph showing experimental setup; (f) drilled Al cast block.

form of fibrous crystals typical of a modified structure represent the main microstructural feature observed. It will also be noted that the iron precipitates in the form of the coarse α-Fe phase, which is always seen to occur within α-Al dendrites, indicating that it corresponds to a predendritic reaction and thus tends to nucleate in the liquid alloy prior to solidification. The copper phase, on the other hand, may be seen mainly as small pockets of the block-like Al_2Cu

Table 2. Cutting Parameters Applied for Machinability Testing

Parameters	Drilling	Tapping
Speed	234.5m/min or 11000rpm.	9.57m/min or 400rpm.
Diameter	Solid carbide "K20" drills: 6.5mm	TiN-coated HSS cutting taps, M8*1.25 UNC. 2B
Tolerance	m7	H4/H5
Depth of hole	Length of cut $\leq 4.5\times$D (28.38mm)	Length of cut $\leq 3\times$D (20.76mm)
Feed rate	1.117m/min	0.56m/min
Coolant	Synthetic metalworking fluid concentrate CIMTECH® 310 (5% cutting fluid + 95% liquid)	

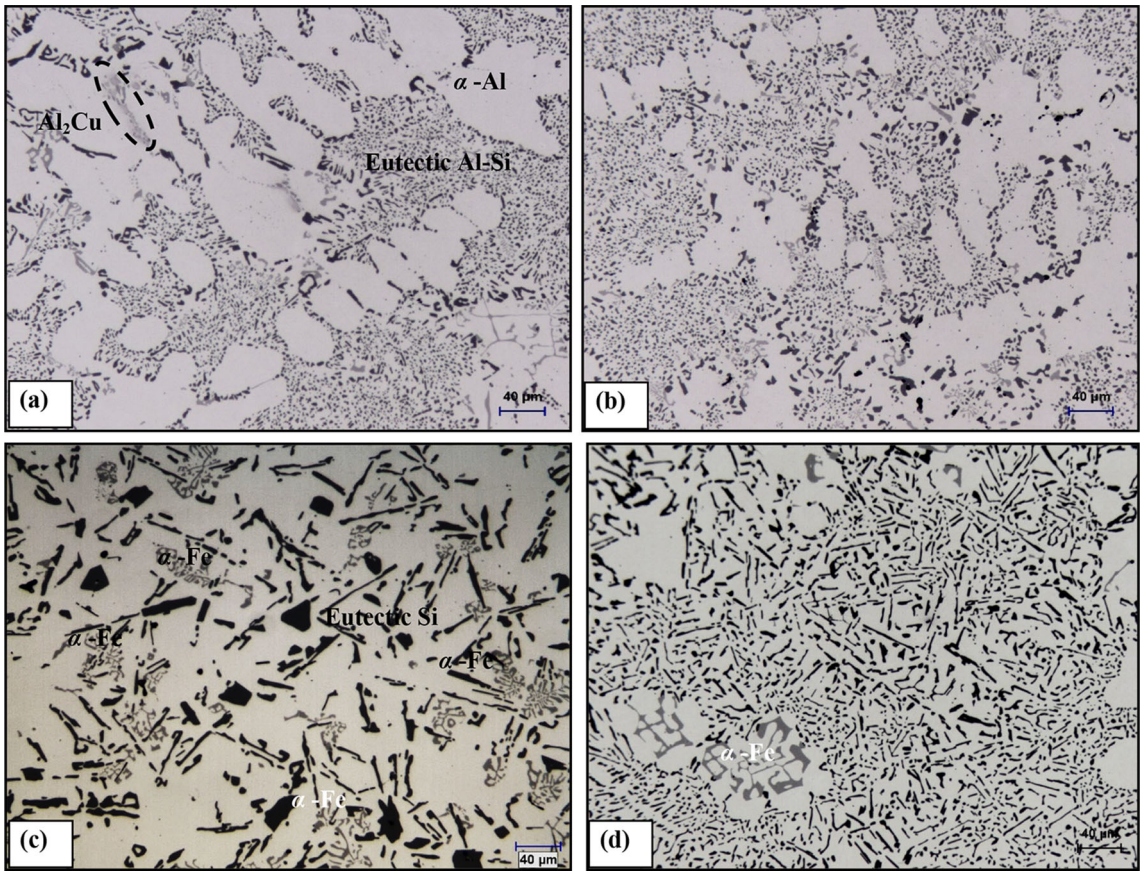

Figure 2. Optical micrographs showing the effects of Sn, Bi, and Pb additions on the microstructure of heat-treated 396 alloys in: (a) M1 base alloy; (b) M2 (M1 + 0.15% Sn); (c) M7 (M1 + 0.5% Bi); and (d) M8 (M1 + 0.8% Pb) alloys.

phase nucleating either within the aluminum matrix or at the interface of such preexisting constituents as Si or intermetallic particles. The platelet-like β-Fe phase was not in evidence because of the higher Mn/Fe ratio in the 396-M1 alloy ($\sim$1.17); this ratio promotes the formation of the α-Fe phase at the expense of the β-Fe phase.

Figure 2a–d shows the effects of Sn, Bi, and Pb additions on the microstructure of 396 alloys. Table 2 summarizes the eutectic Si-particle characteristics obtained for the alloys investigated. It will be observed that the addition of 0.15% Sn to the M1 alloy, producing M2 alloy, leads to a slight coarsening of the eutectic Si particles, as seen in Figure 2b, which illustrates that the average roundness and

Table 3. Summary of the Eutectic Si-particle Measurements for the Alloys Studied

Alloy code	Particle area (μm²)		Particle length (μm)		Roundness ratio (%)		Aspect ratio		Density (particles/ mm²)
	Av*	SD**	Av	SD	Av	SD	Av	SD	
M1	4.30	6.51	2.96	2.49	70.00	17.30	1.77	0.784	28000
M2	4.72	6.10	3.00	2.22	65.00	16.20	1.69	0.681	23000
M7	40.60	60.80	13.30	13.70	30.70	18.20	3.39	2.07	4500
M8	11.6	12.9	6.18	5.18	45.60	20.50	2.40	1.44	15000

*Average value, ** Standard deviation

density, in particles/mm^2, decrease by ~7% and ~18%, respectively. The corresponding data also reveal that the addition of 0.15% Sn has little effect on the values of the average particle area, particle length, and aspect ratio compared to the M1 alloy, as shown in Table 3.

The addition of 0.5% Bi to the 396 alloy counteracts the modifying effect of Sr, as is clearly shown in Figure 2c, leading to a noticeable coarsening of the Si particles. The eutectic Si-particle analysis of the average particle area showed a jump in this parameter from 4.30μm^2 in the M1 alloy to 40.60μm^2 in the M7 alloy. Also, particle length increased from 2.96μm in the M1 alloy to 13.30μm after the addition of Bi. On the other hand, the average roundness and density decrease significantly, by 56% and 84%, respectively. The impairment of Sr modification in the presence of Bi may be interpreted in terms of a Bi–Mg–Si interaction and/or a Bi–Sr interaction. It is possible that a ternary compound, Bi_2Mg_2Sr, and/or the binary compounds, Bi_3Sr, BiSr, Bi_2Sr_3, and $BiSr_2$, may form, resulting in a reduction in the amount of Sr available for modification.

The addition of 0.8% Pb to the M1 alloy is illustrated in Figure 2d; a coarser and partially modified eutectic structure is thus to be observed with this addition; the modification level corresponds to that of a class 3 type, namely partial modification. The corresponding data, see Table 3, on the average particle area, particle length, and aspect ratio, respectively, show an increase from 4.30μm^2, 2.96 μm, and 1.77 in the M1 alloy to 11.6μm^2, 6.18μm, and 2.40 in the M8 alloy. On the other hand, the average roundness and density decrease from 70% and 28000 particles/mm^2 in the M1 alloy to 45.6% and 15000 particles/mm^2, respectively, in the M8 alloy.

The size, shape, and distribution of free-machining particles are of critical importance in the machining of Al–Si casting alloys. Figure 3a shows a backscattered image, obtained at high magnification, of the heat-treated M2 alloy containing 0.15% Sn in which the precipitation of Sn in the form of white phase particles may be observed. It should be noted that, according to atomic number sequence, these white particles observable in the backscattered images of the matrix are β-Sn and that the distribution of the β-Sn particles is not uniform; rather, they appear as small clusters. This figure shows also that the tin particles, or β-Sn, precipitate within the grey Al_2Cu particles and also as tiny Mg_2Sn particles on the eutectic Si particles; high Sn concentrations may be observed in Figure 3b for the β–Sn particles shown in Figure 3a. The corresponding EDX spectrum, as shown in Figure 3c, displays strong reflections due to Sn.

Figure 4a displays a high-magnification backscattered image of the M7 alloy sample containing 0.5% Bi, showing the morphology of Bi-particles precipitated in the alloy; the distribution of Bi and Mg within Bi-containing particles is shown in Figure 4b and c, respectively. The Bi-phase is not observed as an intermetallic compound with Al, since it is independently distributed; this phase is thus not uniformly distributed in Al–Si alloy structures and has a tendency to segregate, forming a coarse phase because of the high wettability of Bi at the grain boundaries. Due to the high atomic number of Bi, it may be detected easily in the form of white particles in the backscattered image. Figure 5a shows a backscattered image of the M8 alloy containing 0.8% Pb at low magnification; in accordance with the high atomic number sequence, the white phase in the matrix is composed of Pb particles, which have precipitated within the α-Fe phase. The corresponding EDX spectrum, as seen in Figure 5b, displays a strong reflection due to the Pb content of the Pb-containing particles.

Hardness and Tensile Properties

The effects of elements having low melting points on the mechanical properties of Al alloys have been reported in various studies. Mohamed *et al.*[29] investigated the effects of trace additions of Sn on the mechanical properties of B319.2 and A356.2 alloys; their results show that the higher ductility of Sn-containing alloys in the as-cast condition may be attributed to the stress–strain state of the matrix material associated with the fine Sn-bearing phase. In a study of the effects of Mg on the mechanical properties of secondary Al–Si–Mg alloys containing 0.1% Sn or 0.2% Pb, it was found that, with an increase in the Mg content

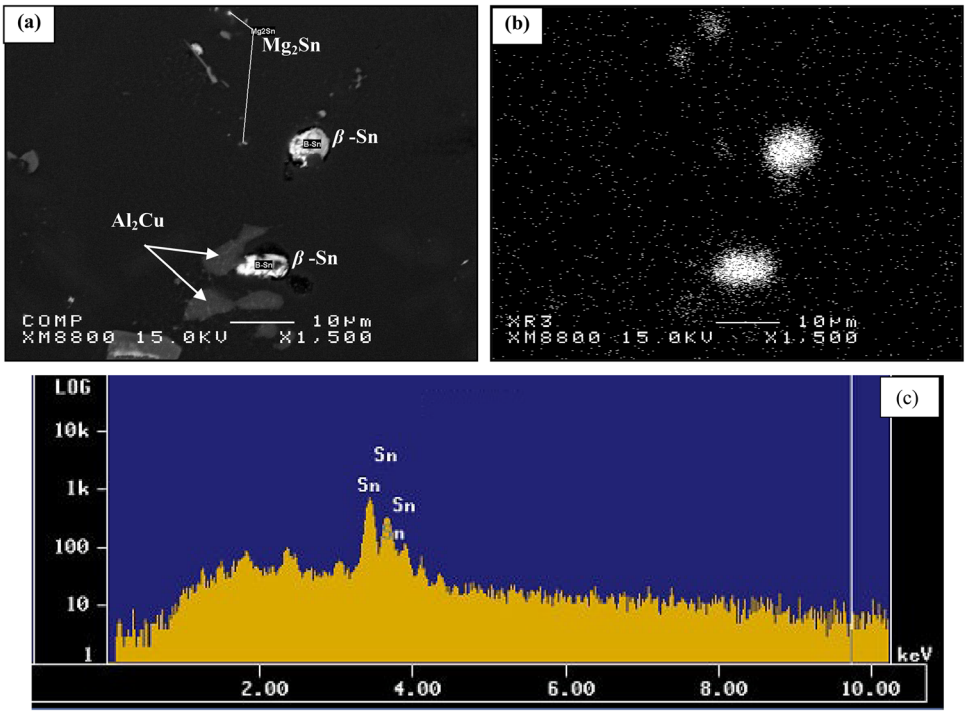

Figure 3. (a) High-magnification backscattered image of the M2 alloy showing precipitation of β-Sn, (b) X-ray image of Sn distribution for the same particles illustrated in (a). (c). EDX spectrum corresponding to β-Sn particles observed in M2 alloy containing 0.15% Sn.

from 0.2 to 0.5–0.8%, the Sn and Pb in the given concentration do not impair the mechanical properties, particularly in the heat-treated condition.[24] On the other hand, Grebenkin *et al.*[30] indicated that Sn and Pb are analogs of Si in electron distribution; these elements are capable of replacing Si in compounds with Mg, which prevents the formation of Mg_2Si or $Al_xMg_5Cu_4Si_4$ hardening phases in Al–Si alloys.

Table 4 provides the relevant data relating to T6 heat-treated mechanical properties; these include the hardness (BHN), yield strength (YS), ultimate tensile strength (UTS), and percent elongation (%El) of the Sr-modified 396 alloys after the addition of Sn, Bi, and Pb. The corresponding hardness data indicate that the M7 alloy containing 0.5% Bi has the highest hardness value compared to the other alloys. On the other hand, the presence of 0.5% Bi in the M7 alloy results in a decrease of YS, UTS, and %El by 10%, 9%, and 34%, respectively. The significant reduction observed in the ductility value of the M7 alloy may be attributed to the effects of the addition of Bi in transforming the structure of the M1 base alloy from a well-modified to a non-modified structure, as shown earlier in the discussion on microstructure. It is important to mention here that the reduction caused in the tensile properties of the M7 alloy, compared to the M1 alloy, may be explained in terms of the Bi–Mg interaction, which consumes the Mg available for the precipitation of Mg-hardening phases.

It has been reported that Bi is a surface active element, and its accumulation near Si or intermetallics may reduce the energy of the system. Most of the Bi particles were connected to intermetallic and Si phase particles, which would result in a deteriorating effect on the mechanical properties of the alloy.[31] It will be observed that the addition of 0.15% Sn causes a marginal reduction in the hardness and tensile properties of the 396-M1 alloy. The same results were observed in the case of the addition of 0.8% Pb.

Machining Behavior

Cutting Forces and Tool Life

A number of Sr-modified, grain-refined, and T6 heat-treated 396 alloys were selected in order to study the effects of the addition of free-machining elements: (i) on the mean total drilling force, (ii) on the mean total drilling moment, and (iii) on the mean drilling power, when based on the mean value of 90 holes; these free-machining elements include Sn, Bi, and Pb. The alloys in question were individually represented by the 396 base alloy, coded M1; 396 + 0.15% Sn, coded M2; 396 + 0.5% Bi, coded M7; and 396 + 0.8% Pb, coded M8, yielding hardness values of 108, 106, 115, and 108 BHN, respectively.

The results obtained from the drilling tests reveal that the mean total drilling force, the mean total drilling moment,

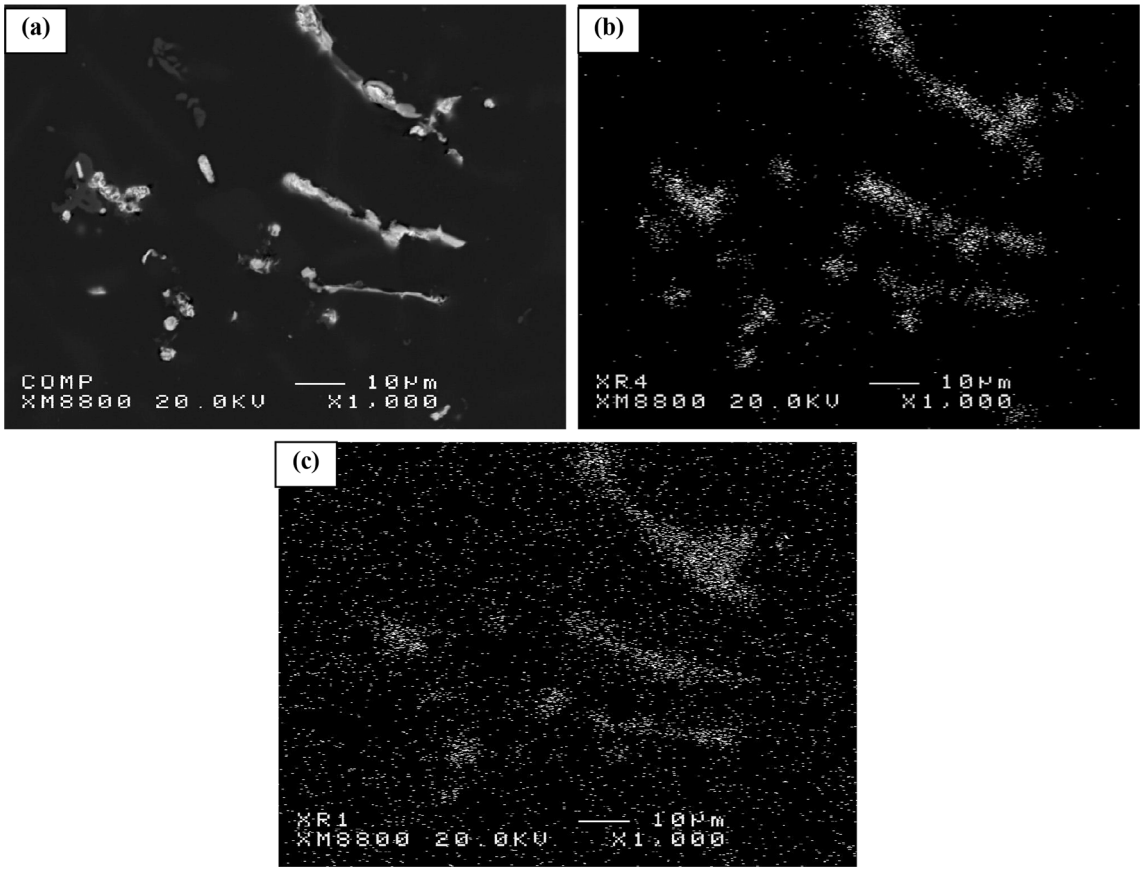

Figure 4. (a) Backscattered image of the M7 (M1 + 0.5% Bi) alloy showing morphology of Bi-containing particles, and X-ray images of (b) Bi and (c) Mg distribution for the same particles illustrated in (a).

and the mean drilling power all increase as the number of holes drilled increases; this form of increase is clear from Figure 6a–c, respectively. It should also be noted that the greatest fluctuation in values in the total drilling forces can generally be observed with a higher number of holes drilled; this analysis agrees with the mean total drilling moment and the mean drilling power of the M1 alloy. The drilling data also suggest that the effects of the addition of free-machining elements on machinability criteria are that the reduction in drilling power is more pronounced than the reduction in total drilling forces. This observation may be explained by the fact that the drilling power responses are mostly susceptible to chip clogging in drill flutes[33], whereas the drilling force is vulnerable to changes in the geometry of the tool cutting edge.[11]

Figure 6a–c shows that the addition of 0.5% Bi to the M1 alloy, thereby creating M7 alloy, improves alloy machinability by lowering the mean total drilling forces and moments, as well as the mean drilling power compared to the M1 alloy. The M7 alloy generated an average of 17% lower drilling forces ranging from 13% to 21% and exhibited an average of 20% lower drilling moment ranging from 24% to 16%, as well as an average 28% less drilling power ranging from 30% to 25% compared to the M1 alloy over the evaluation period of 630 holes. By contrast, the presence of 0.5% Bi in the 396 alloys causes deterioration in drill life, whereas the drill life of the M1 Bi-free alloy decreases from 2160 holes/drill to only 630 holes/drill in the Bi-containing M7 alloy, which corresponds to a reduction in the drill life of ∼71%, as shown in Figure 7. It may be concluded, then, that the Bi-containing M7 alloys exert a negative influence on drill life, although it is observed to exhibit lower drilling forces, moment, and power compared to the M1 base alloy.

The addition of Sn to 396 casting alloys in small but effective amounts of ∼0.15%, thereby producing the M2 alloy, significantly improves the machinability characteristics of these alloys with respect to mean drilling power; which decreases by an average of 17% (ranging from 20% to 13%) compared to the Sn-free M1 alloy, as shown in Figure 6c. On the other hand, the addition of 0.15% Sn to the M1 alloy has some slight effect in decreasing the mean total drilling force as well as the mean total drilling moment, which decrease by an average of 7% and 6%, respectively, over the evaluation period of 2160 holes, as shown in Figure 6a, b.

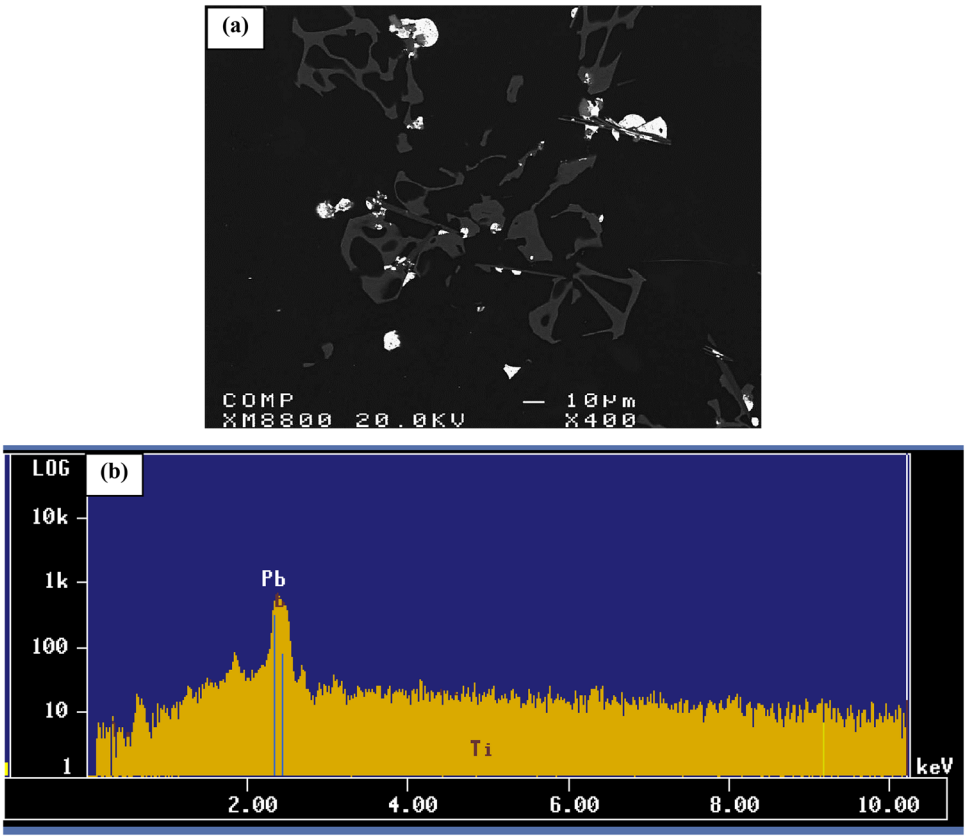

Figure 5. (a) Backscattered image of the M8 (M1 + 0.8% Pb) alloy showing the precipitation of Pb-containing particles (white), (b) EDX spectrum corresponding to Pb-containing particles.

Table 4. Summary of Mechanical Properties for the 396 Alloys Studied

Alloy code	BHN (MPa)	YS (MPa)	UTS (MPa)	El (%)
M1	108 ± 3.56	358.10 ± 1.55	394.04 ± 6.27	0.98 ± 0.12
M2	106 ± 3.19	351.65 ± 2.57	390.54 ± 5.73	1.02 ± 0.15
M7	115 ± 3.76	321.39 ± 3.34	360.61 ± 11	0.65 ± 0.14
M8	108 ± 1.30	335.72 ± 5.76	371.74 ± 6.52	0.93 ± 0.13

During drilling tests, it was also found that the M2 alloy containing 0.15% Sn displayed the same number of holes drilled as in the M1 base alloy, namely 2160 holes/drill, followed by the M8 alloy containing 0.8% Pb reaching 1512 holes/drill, and finally the M7 alloy containing 0.5% Bi, which displayed a noticeable shortening of drill life reaching only 630 holes/drill. Thus, the addition of 0.15% Sn to the 396 alloys has a positive effect on drill life since the Sn-containing alloy yields the longest drill life, *i.e.*, three-and-a-half times that of the Bi-containing alloy, and one-and-a-half times that of the Pb-containing alloy. It should be mentioned here, however, that the Sn-containing M2 alloy requires much higher values of drilling force, moment, and power than are needed by the Bi- and Pb-containing M7 and M8 alloys, respectively.

It is considered that the addition of Pb to aluminum alloys is the method most adequate for improving their machinability values; Pb, however, is not a suitable choice as an additive based on environmental concerns. In this study, the free-machining M8 alloy containing 0.8% Pb displays a reduction in the drilling force, the drilling moment, and in particular the drilling power, which decreased by an average of 80% compared to the Pb-free M1 alloy, as shown in Figure 6c.

The above results show that the machinability of the alloys under investigation was significantly improved by adding small amounts of free-machining elements to the alloy. The effects of free-machining elements may be interpreted by an examination of the alloy microstructure as discussed previously together with an analysis of the existing

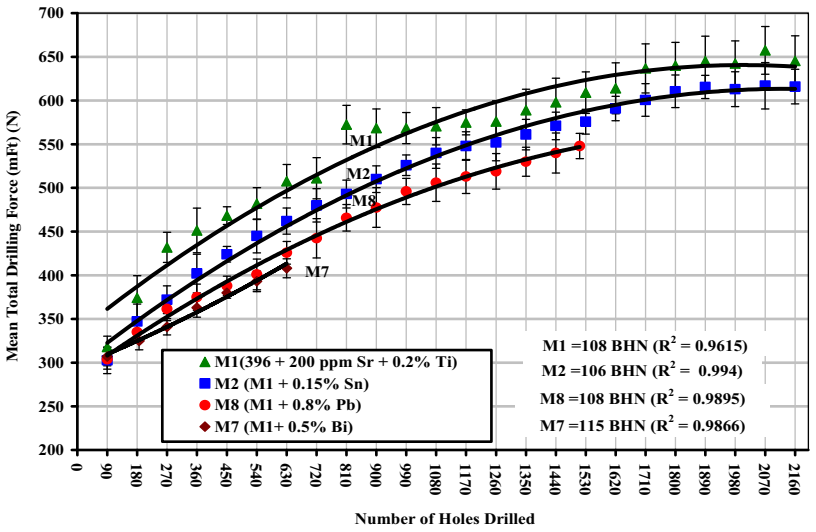

(a)

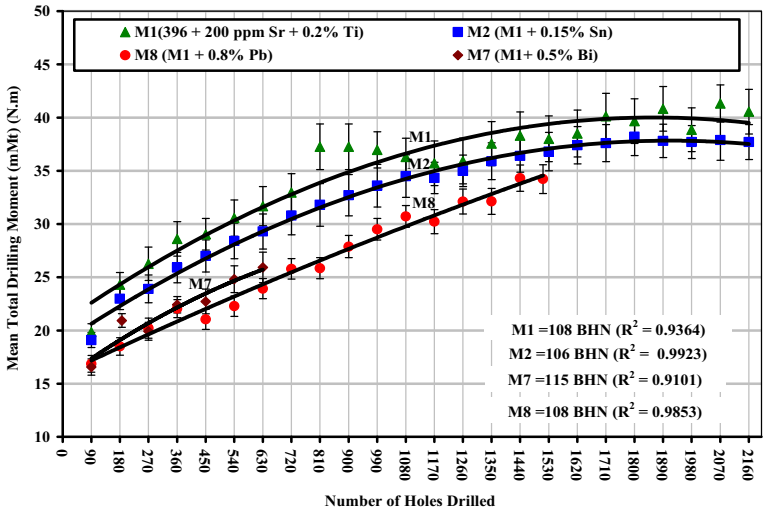

(b)

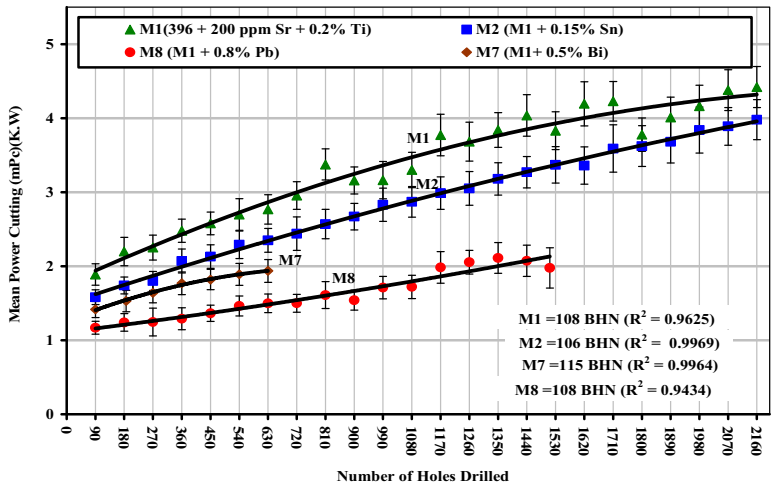

(c)

Figure 6. Effects of adding Sn, Bi, and Pb on the machinability of 396 (M1, M2, M7, and M8) alloys in terms of (a) mean total drilling force; (b) mean total drilling moment; and (c) mean cutting power required for drilling 90 holes.

bibliographic data regarding the effects of these elements on the machinability of the alloys. Thus, the factors involved in reducing the drilling force and moment for the free-machining alloys may be considered in terms of the following: (i) precipitation of free-machining elements in the form of low melting point constituents compared to the aluminum base alloy; (ii) void formation due to the non-uniform deformation of free-machining phases and the Al matrix during the machining process; or (iii) a combination of these two events.

With regard to the Sn-containing M2 alloy, it was found that the Sn additive tends to precipitate in the elemental form at a low melting point of 232 °C, being significantly lower than it is for the Al matrix. It is presumed that Sn in its pure form will soften or melt at cutting temperatures, as shown in Figure 8, tending to decrease the ductility of the material in the cutting zone, thereby in turn causing a reduction in cutting forces. This observation is in satisfactory agreement with Smolej *et al.*[16] who substituted Pb and Pb + Bi with Sn in the standard AA2030 and AA2011 alloys, respectively. They reported that, as a result of the extremely limited solubility of the Sn particles in the Al matrix, these particles remain as separate entities dispersed in the matrix; during machining operations, it is believed that the temperature generated in the cutting zone is high enough to soften or even to melt these dispersed entities. Consequently, this melting gives rise to a local loss of material strength and ductility, which in turn leads to the formation of broken chips. Moreover, the low melting elements act as a lubricant during machining, thereby decreasing the friction between chip and tool edge, which then results in a reduction in the cutting force.

With regard to the Bi-containing M7 alloy, it should be kept in mind here that Bi, a highly reactive element, reacts not only with Sr but also with Mg to form the binary compound Bi_2Mg_3 having a very high melting point of 821 °C, which is considerably higher than that for 396 alloys as a whole. This type of Bi–Mg–Sr interaction was also confirmed in research carried out by Elhadad. In fact, Mondolfo [1] stated that the Bi_2Mg_3 compound, once formed, is relatively hard and will attain a high melting point; from this, it may be deduced that Bi additions to Al–Mg alloys do not improve the machinability values. Couper[35] also reported that the effectiveness of adding Bi in enhancing the machinability of Al–Si–Mg alloys was found to be reduced by the loss of Bi in the formation of Bi_2Mg_3 compounds. For further investigation, X-ray mapping was conducted on Bi-containing particles to determine the distribution of Bi, Mg, and Sr, as shown in Figure 9; in this regard, the X-ray images of Bi and Mg distribution in the Bi-containing particles are shown earlier in Figure 4.

The mechanism involved in decreasing the drilling force and moment for Bi-containing alloys may be explained by the fact that when the free-machining phase does not precipitate in the form of a eutectic or low melting point compound such as the Bi phase, it may persist as a discontinuity in the aluminum alloy matrix. Consequently, when the matrix material is being subjected to drilling forces, the Bi-containing phase will tend to react to shear stress in a different manner with respect to its surrounding aluminum alloy matrix, thereby creating voids between them. The continued application of machining forces creates new voids and propagates existing ones until these voids interconnect and machining chips are formed. It may thus be concluded that the addition of Bi decreases the

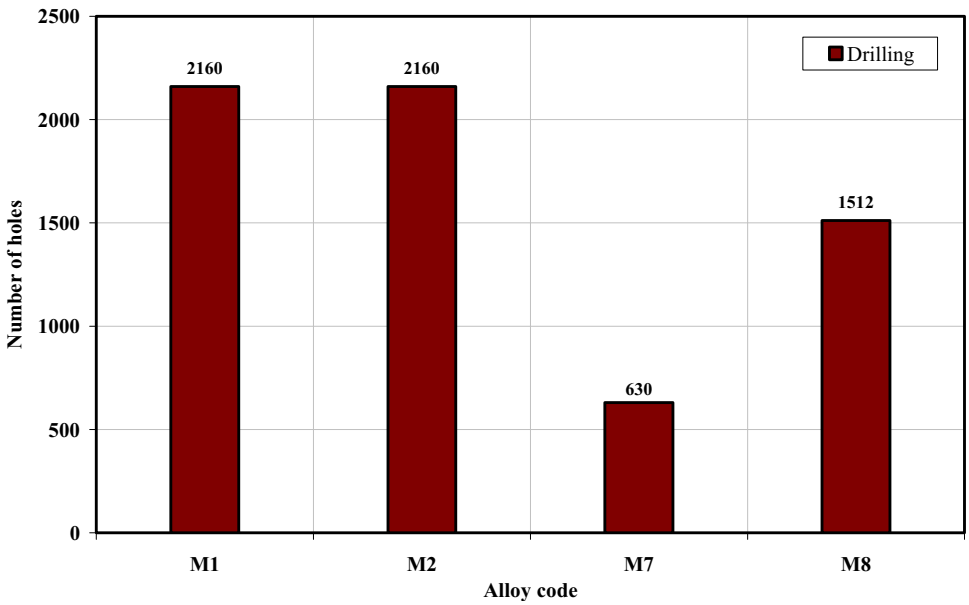

Figure 7. Effects of adding Sn, Bi, and Pb on the drill life of the M1, M2, M7, and M8 alloys in terms of the number of holes drilled.

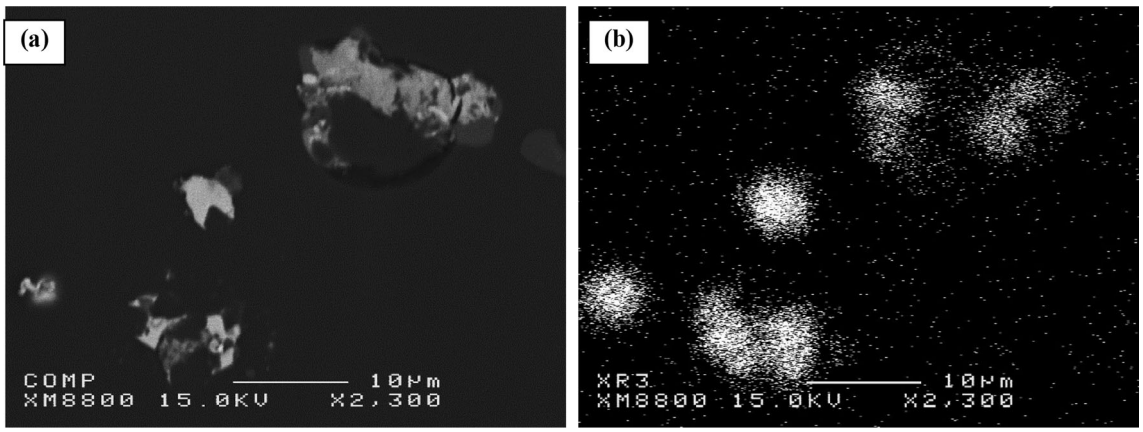

Figure 8. (a) High-magnification backscattered image showing molten Sn particles in the M2 (M1+0.15% Sn) alloy after machining processes, (b) X-ray image of Sn distribution for the same particles illustrated in (a).

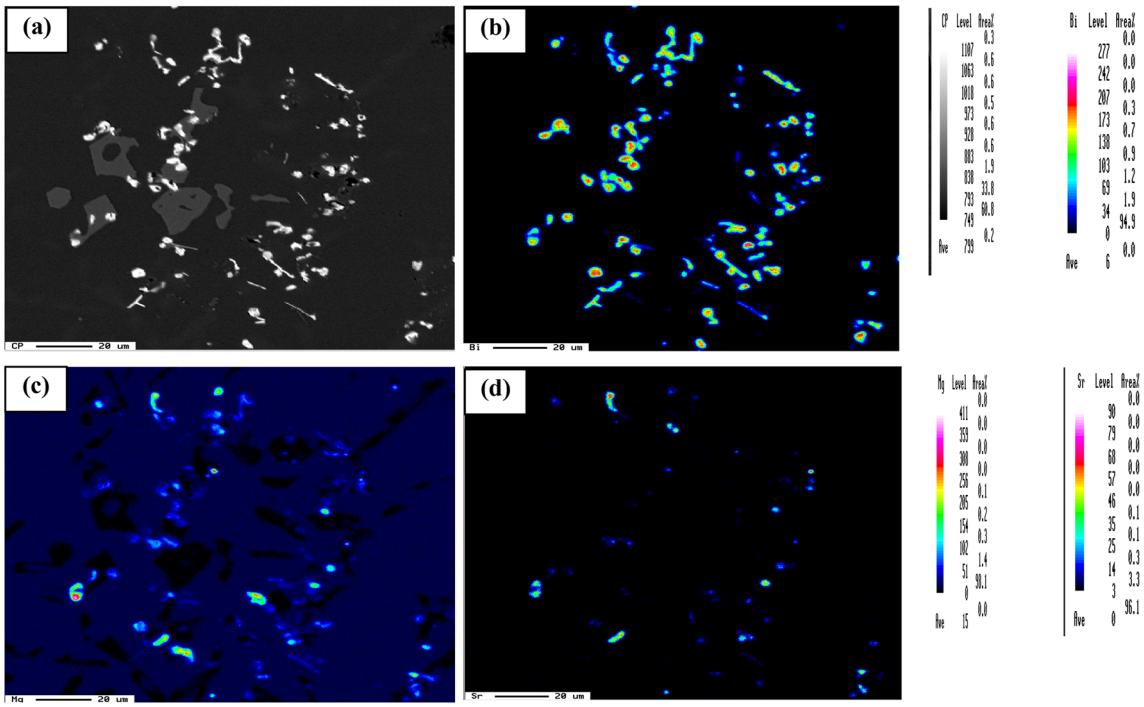

Figure 9. (a) Backscattered image of the M7 alloy showing the precipitation of Bi particles and the corresponding X-ray images of (b) Bi, (c) Mg, and (d) Sr.

drilling force and moment not only through its lubricant effect when part of the Bi particles precipitate in the elemental form but also through its role in decreasing alloy ductility; the Bi-containing M7 alloy, on the other hand, causes a deterioration of the mechanical properties, particularly ductility, which decreases by ∼0.34% compared to the M1 alloy, as shown previously in Table 3.

The presence of 0.5% Bi in the 396 alloys leads to a deterioration of drill life since the drill broke down after only 630 holes although the cutting force results revealed that the Bi is more highly effective than Sn in reducing both drilling force and moment. This noticeable reduction in drill life may be explained by the fact that Bi counteracts the modification effect of Sr through Bi–Mg–Sr interactions, which reduce the amount of free Sr available for Si modification; these interactions are expected to take place in the molten state prior to the precipitation of the eutectic Si. As a result, the Si appears in coarse, acicular form instead of as finely distributed fibrous particles, as evidenced by the optical microstructure shown in Figure 1c. If the eutectic silicon structure is coarse, tool life suffers and results in an increase in the rate of drill wear. Figure 10a and b shows the effects of the addition of Bi on the outer corner of the drill and tool edge after drilling the M7 alloy. As may be seen, wear is visible on the tool edge and at the

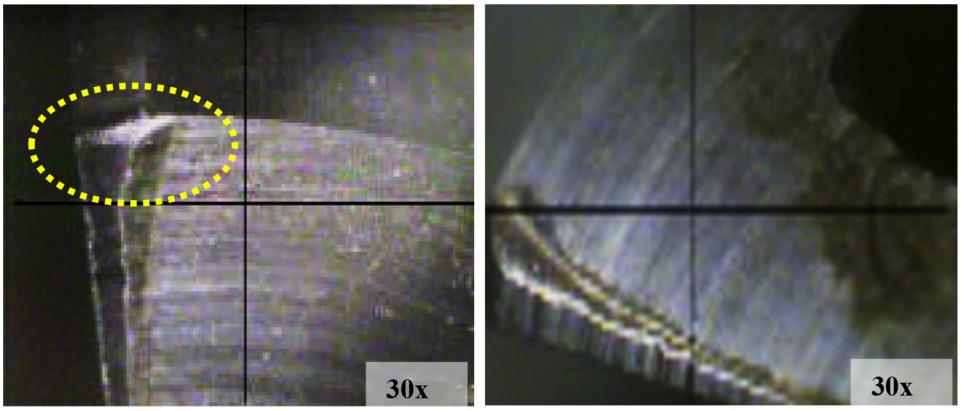

(a) M7- Tool edge after drilling 630 holes. (b) M7- Tool edge after drilling 630 holes.

Figure 10. Photographs showing wear occurring on (a) outer corner and (b) cutting drill lip of the M7 alloy (containing 0.5% Bi) after stripping the BUE in a solution of NaOH.

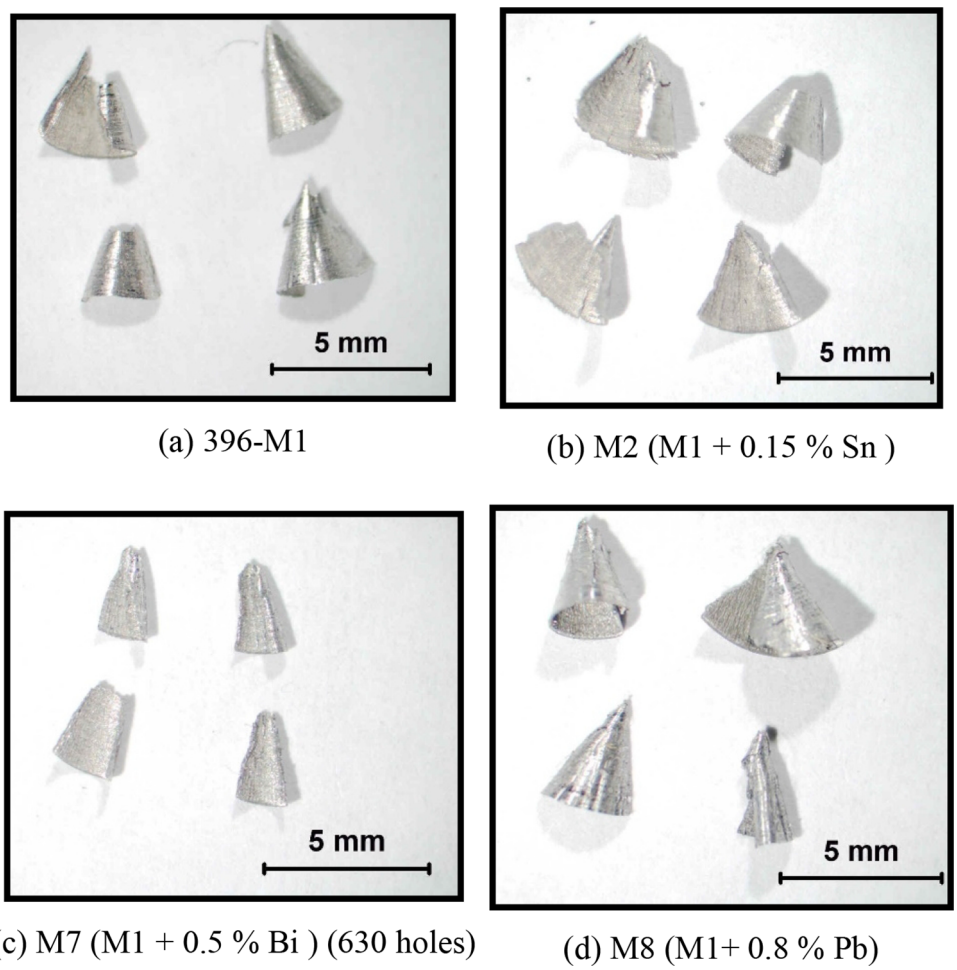

(a) 396-M1 (b) M2 (M1 + 0.15 % Sn)

(c) M7 (M1 + 0.5 % Bi) (630 holes) (d) M8 (M1+ 0.8 % Pb)

Figure 11. Optical micrographs showing the different types of chip obtained for M1, M2, M7, and M8 alloys after drilling the targeted 1080 number of holes (Exception: M7 alloy - 630 holes).

outer cutting corner of the drill. When the corners of the drill are rounded off, the drill then sticks to the workpiece and breaks if the cutting process is not halted in time.

Chip Characterization

The success of a drilling operation depends primarily on the ability to produce chips, which may be readily ejected from the drilled hole. Figure 11b–d shows the effects of Sn, Bi, and Pb on the typical chip formation produced during the drilling of Sr-modified, grain-refined, heat-treated 396 alloys. It was found that the fan shape was by far the predominant form and that it is considered to be the ideal chip for the greater number of drilling applications. Most references in the literature indicate that free machinability is due to the formation of smaller chips. In the current study, chip size was not significantly different after the addition of free-machining elements. The chips were small in the absence of additives, as shown in Figure 11a, and did not become obviously smaller after the inclusion of additives. The Bi-containing M7 alloy, however, produces finer chips of a fan shape than were observed in the alloys under study previously, as shown in Figure 11c. These results were supported by the data obtained after applying the chips-per-gm criterion, as provided in Figure 12. The corresponding data show that the chip breakability of the Bi-containing M7 alloy excelled by an increase of 35% in the number of chips per gram compared to the M1 base alloy.

Conclusions

The following conclusions may be formulated from experiments conducted with a view to studying the influence of Pb, Bi, and Sn additions on the machinability characteristics of Sr-modified, grain-refined, and T6 heat-treated 396 cast alloys.

1. The Bi-containing alloys have a detrimental influence on drill life, although they are observed to exhibit lower drilling forces compared to the M1 base alloys. The significant reduction in drill life may be explained by the fact that the presence of 0.5wt% Bi leads to noticeable coarsening of the Si particles. Moreover, the effectiveness of adding the low melting point Bi for the purpose of enhancing machinability is reduced by the loss of Bi in the formation of the high melting point Bi_2Mg_3 phase.
2. The addition of 0.15wt% Sn to the 396 alloy has a beneficial effect on the tool life of carbide drills. Such an effect may be ascribed to the precipitation of β-Sn particles having a low melting point. In addition, these β-Sn particles are smaller and more uniformly distributed in comparison with the Bi particles in the Bi-containing alloys.
3. Lead is not a suitable choice as an additive because of environmental concerns. Bismuth also has several detrimental effects associated with its presence in the Al–Si alloys, including the formation of high melting point Bi_2Mg_3 phase. Bismuth also interacts with Sr, which is required for Si modification. Thus, of the free-machining

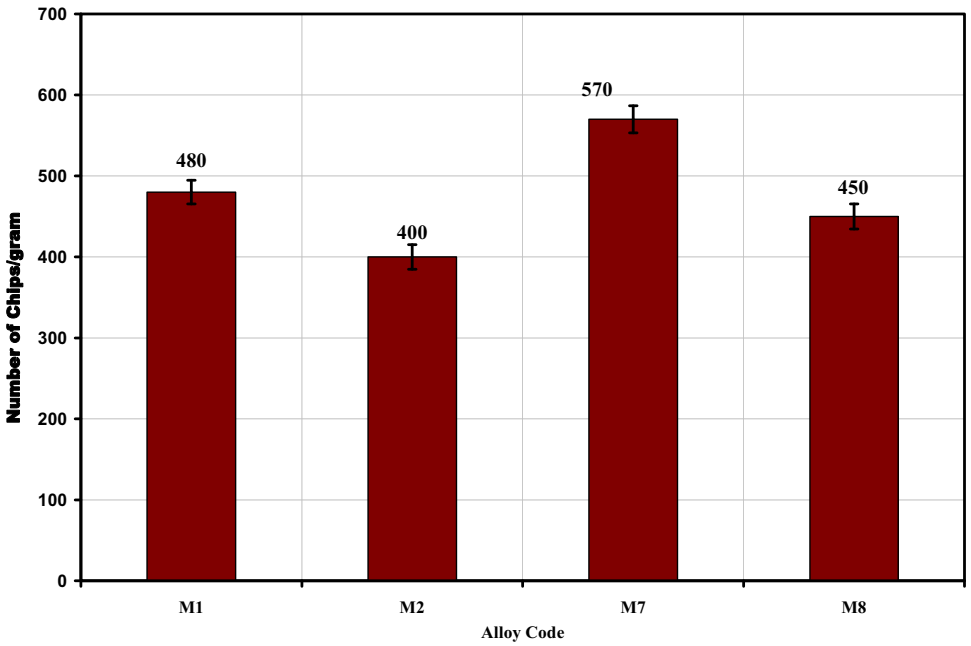

Figure 12. Effects of Sn, Bi, and Pb on chip breakability in terms of the chips-per-gram criterion for the alloys investigated.

elements tested, Sn is the most promising in the context of improving the alloy machinability.

4. A visual examination of the chips reveals that the fan shape was by far the predominant form and that it is considered to be the ideal chip for the greater number of drilling applications. The Bi-containing alloy, however, produces finer chips of a fan shape than were observed in the alloys under study, as evidenced by the data obtained after applying the chip-per-gm criterion.

REFERENCES

1. P. Zhang, L. Zhanqiang, J. Du, G. Su, Correlation between the microstructure and machinability in machining Al–(5–25)wt. %Si alloys. Proc. Inst. Mech. Eng. Part B J. Eng. Manuf. (2020). https://doi.org/10.1177/0954405420911275
2. S.S. Ahn, P. Sharief, J.M. Koo, C.H. Baeg, Enhancement of the mechanical properties in Al–Si–Cu–Fe–Mg alloys with various processing parameters. Materials (2018). https://doi.org/10.3390/ma11112150
3. R.B. Soares, A.M.P. De Jesus, R.J.L. Neto, B.A. Chirita, Comparison between cemented carbide and PCD tools on machinability of a high silicon aluminum alloy. J. Mater. Eng. Perform. (2017). https://doi.org/10.1007/s11665-017-2870-9
4. G. Cordeiro, Q.M. Saraiva, J.R.G. Carneiro, I.Â. Santos, New milling methodology for sealing planes in AlSi9Cu3(Fe) alloy machined with PCD tool. Int. J. Adv. Manuf. Technol. **113**, 1–13 (2021). https://doi.org/10.1007/s00170-021-06843-8
5. Z. Kang, Y. Fu, D.M. Kim, H.E. Joe, From macro to micro, evolution of surface structures on cutting tools: a review. JMST Adv. (2019). https://doi.org/10.1007/s42791-019-0009-x
6. Ş Bayraktar, F. Afyon, Machinability properties of Al–7Si, Al–7Si–4Zn and Al–7Si–4Zn–3Cu alloys. J. Braz. Soc. Mech. Sci. Eng. (2020). https://doi.org/10.1007/s40430-020-02281-x
7. M. Barzani, A.A.D. Sarhan, S. Farahany, R. Singh, Effect of strontium on surface roughness and chip morphology when turning Al-Si cast alloy using carbide tool insert. Int. J. Mech. Prod. Eng. **3**, 36–39 (2015)
8. P. Zhang, Z. Liu, J. Du, Correlation between the microstructure and machinability in machining Al–(5–25) wt% Si alloys. Proc. Inst. Mech. Eng., Part B: J. Eng. Manuf. (2020). https://doi.org/10.1177/0954405420911275
9. P. Ma, Y. Jia, K.G. Prashanth, Z.S. Yu, Effect of Si content on the microstructure and properties of Al-Si alloys fabricated using hot extrusion. J. Mater. Res. (2017). https://doi.org/10.1557/jmr.2017.97
10. RI Nur, MA Suyuti, TA Susanto (2017) Optimizing Cutting Conditions on Sustainable Machining of Aluminum Alloy to Minimize Power Consumption, Preface: The 3rd International Conference on Engineering, Technology and Industrial Application (ICETIA), AIP Conference Proceedings 1855 010001, Doi: https://doi.org/10.1063/1.4985445
11. B. Akÿuz, Effect of Si content on machinability of Al-Si alloys. Kovove Mater **55**, 237–244 (2017). https://doi.org/10.4149/km20174237
12. M.M. Barzani, A.A.D. Sarhan, S. Farahany, S. Ramesh, I. Maher, Investigating the Machinability of Al–Si–Cu cast alloy containing bismuth and antimony using coated carbide insert. Measurement **62**, 170–178 (2015)
13. S.-S. Ahn, S. Pathan, J.-M. Koo et al., Enhancement of the mechanical properties in Al–Si–Cu–Fe–Mg alloys with various processing parameters. Materials **11**, 2150 (2018). https://doi.org/10.3390/ma11112150
14. T.A. Costa, M. Dias, L.G. Gomes, O.L. Rocha, A. Garcia, Effect of solution time in T6 heat treatment on microstructure and hardness of a directionally solidified Al-Si-Cu alloy. J. Alloys Compd. **683**, 485–494 (2016)
15. A.M.A. Mohamed, F.H. Samuel, A review on the heat treatment of Al-Si-Cu/Mg casting alloys.In Heat Treatment-Conventional and Novel Applications; InTech: Rijeka, Croatia, 2012.
16. M. Hamed, Y. Zedan, A.M. Samuel, H.W. Doty, F.H. Samuel, Effect of tool quality on the machinability characteristics of Al-Cu and Al-Si cast alloys. Int. J. Adv. Manuf. Technol. **106**, 1317–1326 (2020)
17. J. Xing, Y. Owada, T. Anami, Effects of Si content on the tensile strength and machinability of Al-Mg-Si-Cu-Mn-Cr alloys. Mater. Sci. (2016). https://doi.org/10.4028/www.scientific.net/MSF.877.141
18. M. Uludağ, Şakir Yazman, D. Dispinar et al., Relationship between machinability microstructure and mechanical properties of Al-7Si alloy. Mater. Sci. (2018). https://doi.org/10.1520/JTE20170083
19. Ş Bayraktar, Dry cutting: a sustainable machining technology. Engineering (2021). https://doi.org/10.1016/B978-0-12-818115-7.00004-3
20. S. Zaima, Y. Takatsuji, M. Iio, Effect of Tin on the machinability of aluminum silicon alloy castings. J. Japan Inst. Light Metals **108**, 556–567 (1970)
21. C.J. Machovec, G.E. Byczynski, J.W. Zindel, L.A. Godlewski, Effect of Bi-Sr Interactions on Si Morphology in a 319-Type Aluminum Alloy. AFS Trans. **108**, 439–444 (2000)
22. H. Bichsel, Bismuth as an alloying element in aluminum alloys. Bull. Bismuth Inst., Bull. **19**, 2–3 (1978)
23. J.-I. Cho, C.R. Loper Jr., Limitation of bismuth residual in A356.2 Al. AFS Trans. **108**, 359–367 (2000)

24. P. Fiorini, G. Giordano, Effect of Zn and Bi addition on precipitation process after quenching and cold working Al-6Mg. Metals Technol. **10**(2), 52–56 (1983)
25. J.M. Dasch, C.C. Ang, C.A. Wong, R.A. Waldo, D. Chester, Y.T. Cheng, The effect of free-machining elements on dry machining of B319 aluminum alloy. J. Mater. Process. Technol. **209**, 4638–4644 (2009)
26. O. Wouters, JTh.M. de Hosson, Lead induced intergranular fracture in aluminum alloy AA6262. Mater. Sci. Eng., A **361**, 331–337 (2003)
27. Jorstad, J.L., "Influence of Aluminum Casting Alloy Metallurgical Factors on Machinability," Society of Automotive Engineers, 400 Commonwealth, PA.15096, 15 pages (1980).
28. Alabi, M.M., Amherst, N.Y., "Hypo-Eutectic Aluminum-Silicon Alloy Having Tin and Bismuth Additions," U.S. Patent, No 5,122,208, Granted 1992.
29. A.M.A. Mohamed, F.H. Samuel, A.M. Samuel, H.W. Doty, S. Valtierra, Precipitation of Tin in Cast 319 and 356 aluminum alloys. AFS Trans. **115**, 15 (2007)
30. V.S. Grebenkin, T.V. Silchenko, A.A. Gorshkov, I.Y. Dzykovich, Effect of magnesium on the distribution of tin and lead in Al-Si alloys. Metals Sci. Heat Treat. **3**, 50–54 (1972)
31. P. Chen, A.T. Alpas, Mechanical properties and machinability of an aluminum-16 wt% silicon alloy modified by 0.5 and 1.0 wt% Bismuth. AFS Trans. **118**, 12 (2010)
32. H. Barakat, Y. Zedan, A.M. Samuel, H.W. Doty, S. Valtierra, F.H. Samuel, Effect of metallurgical parameters on the drilling and tapping characteristics of aluminum cast alloys. Int. J. Adv. Manuf. Technol. **105**, 1357–1370 (2019)
33. A. Smolej, B. Breskvar, M. Soković, V. Dragojević, E. Slaček, Properties of aluminum free-cutting alloys with Tin, Part II. Aluminum **78**, 388–391 (2002)
34. Elhadad, S., "Effect of Trace Elements on the Microstructure and Porosity Formation in 319 Type Al-Si-Cu Alloys," M.Sc. Dissertation 2003, Université du Québec à Chicoutimi, Chicoutimi, QC, Canada
35. Couper, M.J., "6XXX Series Aluminum Alloys," U.S. Patent, No. 6,364,969B1, Granted 2002
36. A.M.A. Mohamed, A.M. Samuel, F.H. Samuel, H.W. Doty, S. Valtierra, Precipitation of Tin in Cast 319 and 356 aluminum alloys. AFS Trans. **151**, 105–119 (2007)
37. Mohamed, A.M.A., F.H. Samuel, A.M. Samuel and H.W. Doty, *Influence of Additives on the Microstructure and Hardness of Al-10.8%Si Near-Eutectic Cast Alloy*, in *7th Arab Foundry Symposium - ARABCAST, Egypt*. 2008
38. A.M.A. Mohamed, F.H. Samuel, A.M. Samuel, H.W. Doty, S. Valtierra, Influence of tin addition on the microstructure and mechanical properties of Al-Si-Cu-Mg and Al-Si-Mg casting alloys. Metall. Mater. Trans. A: Phys. Metallurgy Mater. Sci. **39A**, 490–501 (2008)
39. M.M. Tash, Effect of metallurgical parameters on the machining behavior of 356 and 319 alloys (Drilling and tapping study), PhD Thesis, UQAC, Quebec, Canada, 2005